Establishing an upper bound on contact resistivity of ohmic contacts to *n*-GaN nanowires

2014 Semicond. Sci. Technol. 29 054005

(http://iopscience.iop.org/0268-1242/29/5/054005)

IOP Publishing Semiconductor Science and Technology
Semicond. Sci. Technol. **29** (2014) 054005 (7pp) doi:10.1088/0268-1242/29/5/054005

Establishing an upper bound on contact resistivity of ohmic contacts to *n*-GaN nanowires*

Paul Blanchard, Kris A Bertness, Todd Harvey and Norman Sanford

National Institute of Standards and Technology, 325 Broadway, Boulder, CO 80305, USA

E-mail: paul.blanchard@nist.gov

Received 13 November 2013, revised 27 January 2014
Accepted for publication 14 February 2014
Published 1 April 2014

Abstract

Contact resistivity ρ_c is an important figure of merit in evaluating and improving the performance of electronic and optoelectronic devices. Due to the small size, unique morphology, and uncertain transport properties of semiconductor nanowires (NWs), measuring ρ_c of contacts to NWs can be particularly challenging. In this work, Si-doped *n*-GaN NWs were grown by molecular beam epitaxy. Four-contact structures with 20 nm Ti/200 nm Al contacts were fabricated on individual NWs by photolithography, and the contacts were annealed to achieve ohmic behavior. Two-point resistances R_{23} and four-point collinear resistances $R_{23\text{collinear}}$ were measured between the middle two contacts on each NW. These resistances were then modeled by taking into account the non-uniform distribution of current flow along the length of each contact. Contrary to the assumption that the resistance difference $R_{23}-R_{23\text{collinear}}$ is equal to the total contact resistance R_c, the distributed-current-flow contact model shows that $R_{23}-R_{23\text{collinear}} \ll R_c$ when ρ_c is sufficiently small. Indeed, the measured $R_{23}-R_{23\text{collinear}}$ was so small in these devices that it was within the measurement uncertainty, meaning that it was not possible to directly calculate ρ_c from these data. However, it was possible to calculate an upper bound on ρ_c for each device based on the largest possible value of $R_{23}-R_{23\text{collinear}}$. In addition, we took into account the large uncertainties in the NW transport properties by numerically maximizing ρ_c with respect to the uncertainty range of each measured and assumed parameter in the contact model. The resulting upper limits on ρ_c ranged from 4.2×10^{-6} to 7.6×10^{-6} Ω cm^2, indicating that 20 nm Ti/200 nm Al is a good choice of ohmic contact for moderately-doped *n*-GaN NWs. The measurement and numerical analysis demonstrated here offer a general approach to modeling ohmic contact resistivity via NW four-point measurements.

Keywords: gallium nitride, nanowires, contact resistivity

(Some figures may appear in colour only in the online journal)

1. Introduction

Because of their unique morphology and high crystalline quality [1, 2], GaN nanowires (NWs) are an excellent material from which to develop the next generation of electronic and optoelectronic nano-scale devices. A variety of devices based on GaN NWs have been demonstrated over the past decade, from transistors and sensors to LEDs [3–9]. In order to optimize such devices, robust and well-characterized ohmic contacts are essential. Contact resistivities of Ni/Au [10] and Ti/Au [11, 12] contacts to *n*-GaN NWs have been reported. However, these analyses do not take into account NW surface depletion or contact transfer length, both of which can be important factors in less heavily doped material. In this report, we use a distributed current flow contact model and numerical maximization to establish an upper bound on contact resistivity

* Contribution of the US government, not subject to copyright.

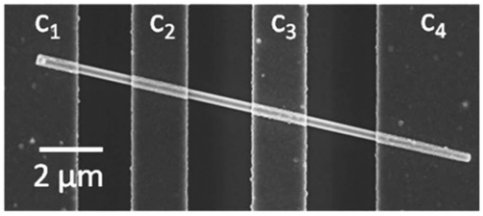

Figure 1. SEM image of a typical four-contact GaN NW device.

of Ti/Al ohmic contacts to individual *n*-GaN NWs grown by molecular beam epitaxy (MBE).

2. Experimental procedure

2.1. Nanowire growth and device fabrication

The NWs in this study were *n*-type, *c*-axis, single-crystalline GaN:Si grown by catalyst-free MBE. The details of the growth can be found elsewhere [13, 14]. NW lengths were between 13 and 20 μm. We approximate the hexagonal cross section of the NW as a circle with diameter $d_{\mathrm{NW}} \equiv 0.91 \times d_{\mathrm{hexagon}}$, where d_{hexagon} is the distance between opposite vertices of the hexagon [15]. Average diameters d_{NW} were between 210 and 390 nm.

Four-contact devices were fabricated from individual NWs as follows. First, the NWs were removed from their growth substrate via ultrasonic agitation in isopropanol and dispersed on a Si/SiO_2 substrate. Next, the contact pattern was defined via conventional photolithography, and the exposed regions of the NW were subjected to a reactive ion etch O_2 plasma treatment immediately before depositing 20 nm Ti/200 nm Al ohmic contacts [16, 17] by e-beam evaporation. Finally, the excess metal and photoresist mask were lifted off in a solvent, and the devices were annealed for 60 s at 500 °C in 5% H_2/Ar. Figure 1 shows a SEM image of a typical finished four-contact NW device. Control *I–V* measurements on identical contact structures without NWs confirmed that the DC resistance between contacts was too high to measure (>10 GΩ) in the absence of a NW between contacts.

2.2. Electrical characterization

Finished NW devices were wire-bonded to a chip socket and placed in a vacuum chamber in total darkness for electrical characterization. Chamber pressures were less than 2×10^{-4} Pa (1.5×10^{-6} Torr). All devices dwelled under vacuum in darkness for at least 12 h prior to testing. All contacts showed linear *I–V* behavior between −1 and +1 V. In order to estimate the contact resistivity of contacts c_2 and c_3 in these four-point devices, we used two resistance measurements: R_{23} and $R_{23\mathrm{collinear}}$. In the R_{23} measurement, a voltage V_{23} was applied across c_2 and c_3 while the current I_{23} was measured; c_1 and c_4 were left open. The two-terminal resistance was calculated as $R_{23} = (\mathrm{d}I_{23}/\mathrm{d}V_{23})^{-1}$. In the $R_{23\mathrm{collinear}}$ measurement, a voltage V_{14} was applied across c_1 and c_4, and the resulting current I_{14} was measured. Simultaneously, the voltage drop V_{23} across c_2 and c_3 was also measured. The resulting 'collinear' resistance was calculated as $R_{23\mathrm{collinear}} = (\mathrm{d}I_{14}/\mathrm{d}V_{23})^{-1}$. To generate each *I–V* curve, the applied voltage V_{23} or V_{14} was swept in a loop from 0 to +500 mV, +500 to −500 mV, and −500 to 0 mV in steps of 20 mV, subject to a current limit of 50 μA. For each device, at least 40 consecutive sets of *I–V* measurements were taken, where each set consisted of one I_{23} versus V_{23} curve followed by one I_{14} versus V_{23} curve.

Across the eight individual-NW four-contact devices that were fabricated and tested, mean R_{23} values varied from approximately 6.8 to 24.0 kΩ. $R_{23\mathrm{collinear}}$ values were nearly identical to R_{23}; the difference $\Delta R_{23} = R_{23} - R_{23\mathrm{collinear}}$ was between about 28 and 90 Ω in each device. Given that ΔR_{23} is less than 1% of R_{23}, it is reasonable to question whether there is really a measurable difference between R_{23} and $R_{23\mathrm{collinear}}$. However, ΔR_{23} proved to be quite repeatable. As table 2 indicates, the standard deviation of ΔR_{23} from the 40 to 50 sets of *I–V* measurements taken from each device is much smaller than ΔR_{23} itself.

3. Analysis

3.1. Theory of nanowire four-point measurements

At first glance, one might naively assume that $R_{23\mathrm{collinear}}$ is a contact-resistance-free measurement, and that the total contact resistance $R_c = \rho_{\mathrm{c}}(1/A_{c2} + 1/A_{c3}) = \Delta R_{23}$, where ρ_{c} is the contact resistivity, and A_{ci} is the contact area of c_i. However, this assumption fails to take into account the possibility that the current I_{14} can be shunted by the contact metal in c_2 and c_3 as it flows from c_1 to c_4. In a 2005 paper [18], Mohney *et al* demonstrated an elegant method for deriving the distributed current flow along the length of a contact to a semiconductor NW. Following their method, the percentage of I_{14} flowing through the NW and through the metal contacts along the length of a hypothetical NW device in the $R_{23\mathrm{collinear}}$ measurement configuration can be calculated. The result is plotted in figure 2(*a*). In this hypothetical device, up to 80% of the current I_{14} flows through the metal in c_2 and c_3. Because of this current shunting, the contact resistivity may contribute to $R_{23\mathrm{collinear}}$.

Following the distributed current flow model, it can be shown that:

$$R_{23} = R_{\mathrm{NW}} + \frac{\rho_{\mathrm{c}}}{b(2\pi r_{\mathrm{NW3}} L_{t3})}\mathrm{Coth}\left(\frac{L_{c3}}{L_{t3}}\right) + \frac{\rho_{\mathrm{c}}}{b(2\pi r_{\mathrm{NW2}} L_{t2})}\mathrm{Coth}\left(\frac{L_{c2}}{L_{t2}}\right) + R_{\mathrm{series}} \quad (1)$$

$$R_{23\mathrm{collinear}} = R_{\mathrm{NW}} + \frac{\rho_{\mathrm{c}}}{b(2\pi r_{\mathrm{NW3}} L_{t3})}\mathrm{Tanh}\left(\frac{L_{c3}}{2L_{t3}}\right) + \frac{\rho_{\mathrm{c}}}{b(2\pi r_{\mathrm{NW2}} L_{t2})}\mathrm{Tanh}\left(\frac{L_{c2}}{2L_{t2}}\right), \quad (2)$$

where

$$L_{ti} = \sqrt{\frac{\pi r_{\mathrm{udmi}}^{\,2}}{\rho_s}\frac{\rho_{\mathrm{c}}}{b(2\pi r_{\mathrm{NW}i})}} \quad (3)$$

$$R_{\mathrm{NW}} = \frac{\rho_s L_{23}}{\pi r_{\mathrm{ud2}} r_{\mathrm{ud3}}}. \quad (4)$$

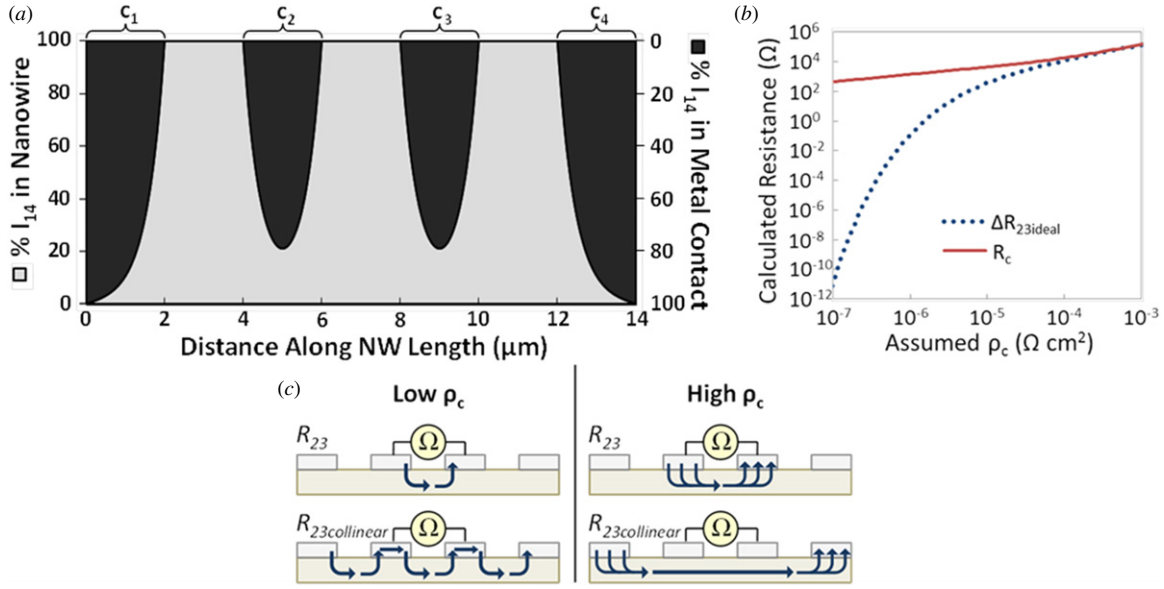

Figure 2. (*a*) Percentage of the total current I_{14} in the nanowire (gray, left axis) and metal contact (black, right axis) calculated for a hypothetical NW device with assumed parameters of $b = 0.75$, $r_{NW} = 150$ nm, $\rho_s = 0.02\ \Omega$ cm, $N_d = 4 \times 10^{17}$ cm^{-3}, $\Phi_b = \Phi_m = -0.1$ V, $L_c = L_{gap} = 2\ \mu$m, and $\rho_c = 5 \times 10^{-6}\ \Omega$ cm^2. (*b*) Calculated values of $\Delta R_{23ideal}$ ($\equiv \Delta R_{23} - R_{series}$) and R_c as a function of assumed ρ_c for the same hypothetical NW device as in (*a*). (*c*) Schematic cross-sectional diagram of current flow in a four-contact NW device. The arrows represent the path that the current takes during a given resistance measurement. At low ρ_c, the current travels through the contact metal along c_2 and c_3 in the $R_{23collinear}$ measurement, resulting in $R_{23collinear} \approx R_{23}$ and $\Delta R_{23ideal} \approx 0$.

Here, ρ_c is the contact resistivity, b is the fraction of the NW circumference that is covered by metal, L_{ti} is the transfer length of contact c_i, L_{ci} is the physical length of c_i, L_{23} is the edge-to-edge gap between c_2 and c_3, and ρ_s is the resistivity of the NW. Because the NW radius r_{NW} ($= d_{NW}/2$) may vary due to taper along the NW length, r_{NW} was measured by SEM at multiple locations in each device; r_{NWi} refers to the NW radius measured at the edge of contact c_i. In (1), an external series resistance R_{series} has been introduced. R_{series} includes any resistance due to the metal leads, wires, and other connections in the current path between the device and the measurement apparatus. R_{series} is not included in the $R_{23collinear}$ measurement because there is zero external current flowing to and from c_2 and c_3 in the collinear configuration.

As has been described in detail in previous work, these *n*-type GaN NWs exhibit some degree of surface depletion due to surface states [15, 19]. By use of Gauss's law and the depletion approximation (which is a valid approximation for the relatively large-diameter NWs considered here), it can be shown that the radius r_{ud} of the undepleted, conductive region of the NW is defined implicitly in terms of the surface potential by:

$$\Phi_{b(m)} = \frac{qN_d}{2\varepsilon}\left(\mathrm{Ln}\left(\frac{r_{ud(m)i}}{r_{NWi}}\right) r_{ud(m)i}{}^2 + \frac{r_{NWi}{}^2 - r_{ud(m)i}{}^2}{2}\right). \quad (5)$$

In (5), q is the electronic charge, N_d is the doping concentration of the NW, and ε is the permittivity of GaN. Φ_b is the surface potential of the bare NW surface, while Φ_m represents the surface potential of the metalized NW surface under each contact. Correspondingly, r_{udi} is the undepleted conducting radius corresponding to Φ_b and r_{NWi} adjacent to c_i, while r_{udmi} is the undepleted conducting radius corresponding to Φ_m and r_{NWi} under c_i.

It is instructive to examine the relationship between the contact resistivity ρ_c and the resistance difference $\Delta R_{23ideal}$, where $\Delta R_{23ideal}$ is simply the measured ΔR_{23} corrected for external series resistance ($\Delta R_{23ideal} \equiv \Delta R_{23} - R_{series}$). Consider the same hypothetical NW device as in figure 2(*a*). By use of (1)–(5), the theoretical resistances $\Delta R_{23ideal}$ and R_c can be calculated for a range of values of ρ_c. The result is plotted in figure 2(*b*). As the plot shows, $\Delta R_{23ideal}$ becomes negligibly small (less than 0.1 Ω) for this hypothetical device when $\rho_c < 10^{-6}\ \Omega$ cm^2, even though $R_c > 100\ \Omega$. In contrast, $\Delta R_{23ideal}$ is very close to R_c when $\rho_c > 10^{-4}\ \Omega$ cm^2.

The relationship between ρ_c, $\Delta R_{23ideal}$, and R_c can be understood conceptually by examining the current flow schematics in figure 2(*c*). At very low ρ_c, the current travels through the contact metal along c_2 and c_3 during the $R_{23collinear}$ measurement. Hence, the current path between c_2 and c_3 is nearly identical in both the R_{23} and $R_{23collinear}$ measurements, which leads to $R_{23} \approx R_{23collinear}$ and $\Delta R_{23ideal} \approx 0$. During the $R_{23collinear}$ measurement at high ρ_c, the path through the NW under the contacts offers a lower resistance than the shunting path, because the shunting path would cross the highly resistive metal/NW interface. Furthermore, at high ρ_c the metal/NW interface resistance becomes large enough to dominate the R_{23} measurement, and that resistance is excluded from $R_{23collinear}$. This leads to $\Delta R_{23ideal} \approx R_c$ at high ρ_c. The precise relationship between $\Delta R_{23ideal}$ and R_c depends on the doping level, surface band bending, and physical dimensions of the NW device, but the hypothetical case calculated here shows that it is not sufficient to simply assume that $\Delta R_{23ideal}$ is equal to the total contact resistance in these devices.

Even though $\Delta R_{23ideal} \neq R_c$, figure 2(*b*) shows that there is a well-defined relationship between $\Delta R_{23ideal}$ and ρ_c. However,

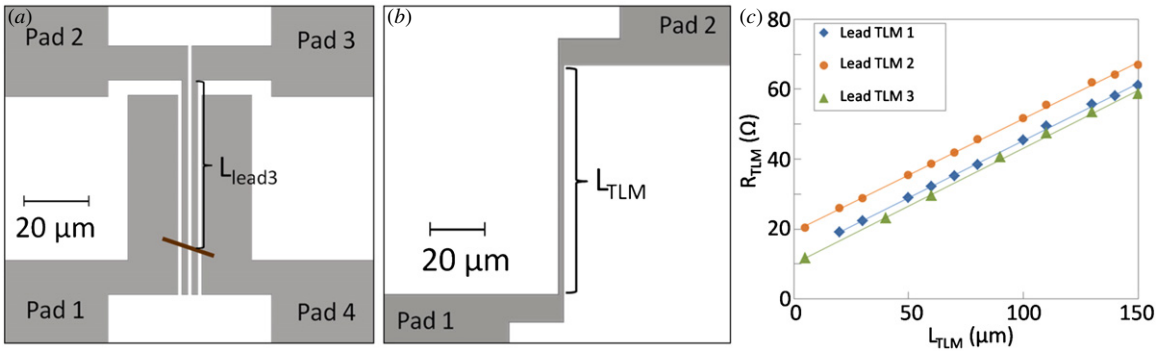

Figure 3. (*a*) Schematic drawing of NW four-point device site. The gray areas represent the Ti/Al contact metal; the white areas represent the substrate. One possible NW position is shown with example lead length L_{lead3} indicated. (*b*) Schematic drawing of a lead TLM device used to measure the resistance of the metal lead. Each TLM die contains up to 12 such devices, across which L_{TLM} varies from 10 to 150 μm. (*c*) R_{TLM} versus L_{TLM} for three different lead TLM die. A linear fit to the data from each die is shown.

ρ_c cannot be directly calculated from the measured ΔR_{23} unless the parameters b, r_{NW}, L_c, N_d, ρ_s, Φ, and R_{series} are known. Of course, $\rho_s = 1/(q\mu N_d)$, where μ is the electron mobility. The physical dimensions can be estimated by SEM inspection, but the NW transport properties remain highly uncertain due to the challenges of measuring N_d, μ, and Φ in the NW morphology. Our approach is therefore to calculate the full range of possible values of ρ_c based on the uncertainty ranges of the physical dimensions and the transport properties. Each ρ_c solution minimizes the total error in (1) and (2) based on the measured R_{23} and $R_{23collinear}$ at a particular set of assumed parameter values from within the uncertainty range of each parameter. The use of both (1) and (2) to find ρ_c, rather than fitting to ΔR_{23} only, ensures that the possible values of N_d, μ, and Φ that are considered are only those consistent with R_{NW}. Even so, ΔR_{23} remains a relevant parameter, as it is included implicitly when calculating ρ_c from (1) and (2).

3.2. External series resistance measurements

Uncertainty ranges for the transport properties can be established based on literature values and our own previous work. However, one remaining unknown is R_{series}. R_{series} is expected to be small, but given that the measured ΔR_{23} is less than 100 Ω, R_{series} could account for a significant portion of ΔR_{23}. R_{series} therefore should not be neglected. One contribution to R_{series} is R_{lead}; R_{lead} is the resistance contributed by the 1.5 μm wide metal leads that connect pads 2 and 3 to the NW. A schematic of a four-point device site is shown in figure 3(*a*). Depending on the position of the NW in the device site, the total lead length L_{lead} can be anywhere from 10 to 130 μm, where $L_{lead} = L_{lead2} + L_{lead3}$.

In order to estimate R_{series}, transmission line measurement (TLM) control samples without NWs were fabricated. In each lead TLM device, a ~1.5 μm wide Ti/Al lead of varying length spans between a pair of contact pads. The fabrication process was identical to that of the four-point NW device contacts. Three separate TLM device die were fabricated, each containing up to 12 TLM devices with lead length L_{TLM} ranging from 5 to 150 μm. An example lead TLM device is shown schematically in figure 3(*b*).

Lead TLM devices were tested under conditions identical to the NW four-point devices. The resulting resistance values R_{TLM} at different lengths L_{TLM} are plotted in figure 3(*c*). The equations for the three fit lines in figure 3 are of the form $R_{TLM} = m \times L_{TLM} + R_{int}$, where m is the lead resistance per unit length and R_{int} is the intercept resistance due to electrical connections in series with the Ti/Al leads. m is fairly consistent at 0.33 ± 0.01 Ω µm^{-1} across the three die. However, R_{int} varies significantly; $R_{int} = 12.6$ Ω for die 1, $R_{int} = 19.2$ Ω for die 2, and $R_{int} = 10.1$ Ω for die 3. It is not clear which of the various connections in the current path between the device and the measurement apparatus is systematically changing between the three dies. Whatever the cause, the uncertainty due to variations in R_{int} is significant.

In the NW devices, R_{series} can be estimated as $R_{series} = R_{lead} + R_{int}$, where $R_{lead} = m \times L_{lead}$ with $m \approx 0.33$ Ω µm^{-1}. After correcting for the lead resistance, the average $\Delta R_{23} - m \times L_{lead}$ was ~29 Ω, which is similar in magnitude to R_{int} from the lead TLM devices. Given that there are only three measurements of R_{int} and that R_{int} varies by nearly a factor of 2, $\Delta R_{23} - m \times L_{lead}$ is effectively within the uncertainty of R_{int}. However, we can say for certain that R_{int} is positive, and that R_{series} does not exceed the measured ΔR_{23}, which means that $0 < R_{int} < \Delta R_{23} - m \times L_{lead}$. This inequality has two consequences. First, it is not possible to establish a non-zero lower bound on ρ_c from these data. The limiting case where the value of $R_{int} \to \Delta R_{23} - m \times L_{lead}$ leads to the lower bound $\Delta R_{23ideal} \to 0$ and $\rho_c \to 0$. Second, it is possible to establish an upper bound on ρ_c; the opposite limiting case where $R_{int} \to 0$ leads to the upper bound $\Delta R_{23ideal} \to \Delta R_{23} - m \times L_{lead}$. Because the relationship between $\Delta R_{23ideal}$ and ρ_c is monotonic, as shown in figure 2(*b*), an upper bound on $\Delta R_{23ideal}$ also places an upper bound on ρ_c.

3.3. Numerical maximization of contact resistivity

In order to establish the upper bound on ρ_c for each device, ρ_c was calculated by numerically solving (1) and (2) for ρ_c in the limiting case where $R_{int} = 0$ (equivalent to $R_{series} = R_{lead} = m \times L_{lead}$). The mobility μ was also treated as a free parameter to be solved for, thus ensuring that ρ_s was consistent with the measured resistances under each set of assumed parameter

Table 1. Parameters and ranges of allowed values used in numerical maximization routine to find the upper bound on ρ_c in NW four-point devices. R_{23} and ΔR_{23} values were restricted to within 2 standard deviations of the mean measured value ($R_{23\text{collinear}}$ was calculated from $R_{23}-\Delta R_{23}$). Uncertainty in length and radius measurements was estimated based on the SEM or optical microscope image resolution. The range in m reflects the variation among the Lead TLM samples. Fractional contact coverage b is based on SEM examination of previous NW devices. Limits on N_d and Φ_b were chosen based on previous and ongoing work [15, 17, 19]. Φ_m is limited to contact barrier heights from which ohmic behavior is possible (based on calculations assuming thermionic field emission at the contact).

Measured parameter	Range of values	Assumed parameter	Range of values
R_{23}	mean(R_{23}) $\pm$ $2\sigma_{R23}$	b	0.5–0.8
ΔR_{23}	mean(ΔR_{23}) $\pm$ $2\sigma_{\Delta R23}$	N_d	1–10 $\times$ 10^{17} cm^{-3}
r_{NW2}, r_{NW3}	Measured value $\pm$ 5 nm	Φ_b	-0.1– -0.3 V
L_{c2}, L_{c3}, L_{23}	Measured value $\pm$ 20 nm	Φ_m	0– -0.3 V
m	0.33 $\pm$ 0.01 Ω μm^{-1}		
L_{lead}	Measured value $\pm$ 5 μm		

Table 2. Results of resistance measurements in four-point devices. R_{23}, $R_{23\text{collinear}}$, and ΔR_{23} are reported as the mean values with errors corresponding to 1 standard deviation. Resistance measurements were repeated between 40 and 50 times. The standard deviation in ΔR_{23} is smaller than the standard deviations in R_{23} and $R_{23\text{collinear}}$ because the fluctuations over time in R_{23} and $R_{23\text{collinear}}$ were correlated with one another. The upper limit on ρ_c is the result of numerical maximization; the total contact resistance corresponding to the maximum ρ_c is also listed.

Device	R_{23} (Ω)	$R_{23\text{collinear}}$ (Ω)	ΔR_{23} (Ω)	R_{lead} (Ω)	Upper limit on ρ_c (Ω cm^2)	Upper limit on R_c (kΩ)
1	24 034 $\pm$ 14	23 990 $\pm$ 17	44 $\pm$ 8	27 $\pm$ 2	7.6 $\times$ 10^{-6}	9.6
2	12 658 $\pm$ 3	12 620 $\pm$ 3	38 $\pm$ 3	19 $\pm$ 2	5.5 $\times$ 10^{-6}	5.4
3	8055 $\pm$ 2	8027 $\pm$ 1	28 $\pm$ 1	19 $\pm$ 2	5.6 $\times$ 10^{-6}	3.4
4	13 650 $\pm$ 8	13 611 $\pm$ 8	39 $\pm$ 3	25 $\pm$ 2	5.1 $\times$ 10^{-6}	5.8
5	9726 $\pm$ 2	9636 $\pm$ 2	90 $\pm$ 1	57 $\pm$ 2	4.2 $\times$ 10^{-6}	3.7
6	10 555 $\pm$ 5	10 498 $\pm$ 5	56 $\pm$ 3	32 $\pm$ 2	5.6 $\times$ 10^{-6}	4.4
7	12 997 $\pm$ 5	12 969 $\pm$ 5	28 $\pm$ 2	17 $\pm$ 2	5.7 $\times$ 10^{-6}	4.3
8	6853 $\pm$ 13	6804 $\pm$ 12	50 $\pm$ 2	42 $\pm$ 2	5.7 $\times$ 10^{-6}	2.8

values. Each of the experimentally measured parameters (R_{23}, $R_{23\text{collinear}}$, r_{NW2}, r_{NW3}, L_{c2}, L_{c3}, L_{23}, m, and L_{lead}) and assumed parameters (N_d, Φ_b, Φ_m, and b) has some uncertainty. The upper bound on ρ_c for each device was found by repeatedly solving (1) and (2) while numerically maximizing the resulting ρ_c with respect to the uncertainty range of each of the measured and assumed parameters. Each calculated ρ_c was considered a valid solution of (1) and (2) if the root sum of squares of the relative errors in (1) and (2) was less than 1 $\times$ 10^{-6}. Numerical maximization of the calculated ρ_c solution was carried out by use of a particle swarm optimization algorithm [20]. The upper limit on ρ_c corresponds to the largest valid ρ_c solution that could be found within the ranges of possible parameter values.

The ranges of values for all parameters are listed in table 1. $R_{23\text{collinear}}$ is not listed. Because fluctuations in R_{23} and $R_{23\text{collinear}}$ over the course of 40 to 50 repeated measurements were correlated with one another, the combined uncertainties in R_{23} and $R_{23\text{collinear}}$ overstate the uncertainty in ΔR_{23}. To correct for this, $R_{23\text{collinear}}$ was calculated as $R_{23}-\Delta R_{23}$ in the maximization routine. In addition, limits were placed on solutions such that a solution was valid only if 200 cm^2 (V s)$^{-1}$ $\leqslant$ μ $\leqslant$ 2500 cm^2 (V s)$^{-1}$; this eliminated solutions that correspond to an unrealistically high or low mobility [15, 21]. Care was taken to err on the side of overestimating the uncertainty when choosing ranges of values; the limits are meant to represent a high-confidence range so that ρ_c is truly an upper limit.

The results are shown in table 2. The upper limit on ρ_c ranged from approximately 4.2 $\times$ 10^{-6} to 7.6 $\times$ 10^{-6} Ω cm^2 among the eight devices. These values are approximately in agreement with ρ_c of quality Ti/Al contacts to n-GaN thin films reported in the literature [22]. The corresponding upper bound on the total combined contact resistance R_c of c_2 and c_3 was between 2.8 and 9.6 kΩ in each device. It is important to remember that ρ_c and R_c may be significantly lower than the upper bound in any or all of these devices. The upper bounds listed here represent the sensitivity limits of this particular experiment.

Although there are plenty of valid ρ_c solutions that correspond to lower μ, it is worth noting that the maximum ρ_c consistently corresponded to mobility at the upper mobility limit of μ = 2500 cm^2 (V s)$^{-1}$. This simply reflects the fact that the maximum possible ρ_c gets larger as the allowed μ gets higher. While μ = 2500 cm^2 (V s)$^{-1}$ is likely (and intentionally) an overestimate of the mobility, any downward revision of this limit in the calculation only decreases ρ_c. Hence, if μ is constrained to lower values, valid ρ_c solutions can still be found, and the upper limit on ρ_c reported here is not violated.

One important assumption in the analysis shown here is that the NW transport and surface properties are constant throughout the section of each NW that includes c_2 and c_3. Hence, the upper bounds reported here are strictly valid only if ρ_c, N_d, μ, Φ_b, and Φ_m are approximately uniform in this region. Position-dependent transport and surface

measurements along the length of individual NWs are subjects of ongoing investigations.

4. Discussion

The four-point measurement and numerical analysis shown here can be applied in a general way to ohmic NW contacts. In fact, the experiment will likely be significantly less complicated in many NW devices, and will allow the possible range of ρ_c to be specified more precisely. In the devices shown here, ΔR_{23} is so small that it is comparable to R_{series}. That is why the lead resistance had to be measured, and only an upper bound on ρ_c could be calculated. In general, however, devices made from other NWs or with different contacts may show much larger ΔR_{23}.

A combination of factors contributes to the relative magnitude of ΔR_{23}. Analysis of (1) and (2) shows that ΔR_{23} becomes larger as the ratio of the contact length to the transfer length L_c/L_t decreases. In general, this means that ΔR_{23} will be larger in devices with higher contact resistivity, shorter contact length, and/or lower NW resistivity. We estimate that L_t in our devices is on the order of 400 nm or less, compared to $L_c \sim 1.5$ μm. However, many NW devices reported in the literature have shorter e-beam lithography (EBL)-defined contacts and significantly higher doping levels, which would lead to higher ΔR_{23} in four-point devices.

There are two advantages to large ΔR_{23}. First, $\Delta R_{23} \gg R_{series}$ means that R_{lead} and R_{int} can be neglected. Secondly, in devices with $\Delta R_{23} \gg R_{series}$, ρ_c can be specified more precisely, because both an upper *and a lower* bound on ρ_c can be calculated. Due to the small ΔR_{23} and relatively large uncertainty due to R_{int} in our devices, the lower limit on $\Delta R_{23ideal}$ was zero, and thus the lower bound on ρ_c was also zero. When $\Delta R_{23} \gg R_{series}$, on the other hand, $\Delta R_{23ideal} \approx \Delta R_{23}$ and the relative uncertainty due to R_{int} is negligible. There can therefore be a non-zero lower bound on $\Delta R_{23ideal}$, and the full range of possible ρ_c can be found by solving (1) and (2) while numerically maximizing (to find the upper bound) or minimizing (to find the lower bound) ρ_c with respect to the uncertainty ranges of the parameters. Hence, larger ΔR_{23} can both simplify and improve the ρ_c measurement.

It is worth noting that in the limit where $L_c \ll L_t$, one can make the approximations that $\mathrm{Coth}(L_c/L_t) \approx L_t/L_c$ and $\mathrm{Tanh}(L_c/2L_t) \approx L_c/2L_t \approx 0$. In the case of $L_c \ll L_t$, subtracting (2) from (1) (with $R_{series} = 0$) thus yields the familiar $\Delta R_{23} \approx R_c \approx \rho_c(1/A_{c2} + 1/A_{c3})$, where the contact area $A_{ci} = b(2\pi\ r_{NWi}\ L_{ci})$. Hence, ρ_c in NW devices with sufficiently short contact length compared to the transfer length can, in principle, be directly calculated from $\Delta R_{23} = \rho_c(1/A_{c2} + 1/A_{c3})$. However, it can be difficult to justify the initial assumption that $L_c \ll L_t$, because ρ_c is not initially known, and the NW transport properties used to calculate L_t are often highly uncertain. It is likely that $\Delta R_{23} = \rho_c(1/A_{c2} + 1/A_{c3})$ is a reasonably good approximation for some NW devices. However, the more general approach shown here of numerically fitting to the distributed-current-flow model allows contacts with relatively shorter transfer length to be evaluated more accurately, and allows the uncertainties to be taken explicitly into account.

5. Conclusions and future work

In summary, four-contact structures with 20 nm Ti/200 nm Al ohmic contacts on individual *n*-GaN NWs were fabricated and tested. The devices were analyzed by use of a distributed current flow contact model. The model shows that the difference ΔR_{23} between the two-terminal resistance and four-point collinear resistance may be orders of magnitude less than the contact resistance R_c. After correcting for lead resistance, the values of $\Delta R_{23} - R_{lead}$ in these devices fell within the uncertainty of the external series resistance due to the measurement apparatus. Because of this uncertainty, it was not possible to establish a non-zero lower limit on ρ_c. However, an upper limit on ρ_c was established by numerically maximizing ρ_c with respect to the uncertainty ranges of the measured and assumed parameters in the contact model. The upper limit on ρ_c ranged from 4.2×10^{-6} to 7.6×10^{-6} Ω cm^2 among the eight devices tested, indicating that ρ_c in these contacts compares favorably with moderately-doped *n*-GaN thin film contacts found in the literature. The measurement technique and numerical analysis demonstrated here offer a general approach to determining the range of possible ρ_c in nanowire contacts, and the broader applicability was discussed.

An excellent extension of the study conducted here would be to decrease the length of contacts c_2 and c_3 to try to increase ΔR_{23}. Unfortunately, the contact leads used here are already the narrowest lines that could be reliably fabricated by the conventional photolithography at our immediate disposal. Significantly narrower contact leads can be fabricated by EBL, and future experiments with EBL-defined contacts of varying length are planned. Even so, it is unclear whether ρ_c in contacts fabricated by EBL would be an accurate representation of ρ_c in contacts fabricated through our usual photolithography process.

References

[1] Bertness K A, Schlager J B, Sanford N A, Roshko A, Harvey T E, Davydov A V, Levin I, Vaudin M D, Barker J M, Blanchard P T and Robins L H 2005 *MRS Proc.* **892** 0892-FF31-03

[2] Schlager J B, Sanford N A, Bertness K A, Barker J M, Roshko A and Blanchard P T 2006 *Appl. Phys. Lett.* **88** 213106

[3] Blanchard P T, Bertness K A, Harvey T E, Mansfield L M, Sanders A W and Sanford N A 2008 *IEEE Trans. Nanotechnol.* **7** 760–5

[4] Aluri G S *et al* 2012 *Nanotechnology* **23** 12

[5] Blanchard P T *et al* 2012 *IEEE Trans. Nanotechnol.* **11** 479–82

[6] Cha H Y *et al* 2006 *Nanotechnology* **17** 1264–71

[7] Sekiguchi H, Kato K, Tanaka J, Kikuchi A and Kishino K 2008 *Phys. Status Solidi* a **205** 1067–9

[8] Stern E *et al* 2005 *Nanotechnology* **16** 2941–53

[9] Wu H Q, Cha H Y, Chandrashekhar M, Spencer M G and Koley G 2006 *J. Electron. Mater.* **35** 670–4

[10] Stern E, Cheng G, Young M P and Reed M A 2006 *Appl. Phys. Lett.* **88** 053106

[11] Ham M H, Choi J H, Hwang W, Park C, Lee W Y and Myoung J M 2006 *Nanotechnology* **17** 2203–6

[12] Hwang J S *et al* 2004 *Appl. Phys. Lett.* **85** 1636–8

[13] Bertness K A, Roshko A, Mansfield L M, Harvey T E and Sanford N A 2007 *J. Cryst. Growth* **300** 94–99

[14] Bertness K A *et al* 2006 *J. Electron. Mater.* **35** 576–80
[15] Sanford N A *et al* 2013 *J. Appl. Phys.* **113** 174306
[16] Yan J, Kappers M J, Barber Z H and Humphreys C J 2004 *Appl. Surf. Sci.* **234** 328–32
[17] Mansfield L, Bertness K, Blanchard P, Harvey T, Sanders A and Sanford N 2009 *J. Electron. Mater.* **38** 495–504
[18] Mohney S E *et al* 2005 *Solid-State Electron.* **49** 227–32
[19] Sanford N A *et al* 2010 *J. Appl. Phys.* **107** 034318
[20] Clerc M and Kennedy J 2002 *IEEE Trans. Evol. Comput.* **6** 58–73
[21] Djeffal F, Arar D, Lakhdar N, Bendib T, Dibi Z and Chahdi M 2009 *Microelectron. J.* **40** 357–9
[22] Luther B P, Mohney S E, Jackson T N, Khan M A, Chen Q and Yang J W 1997 *Appl. Phys. Lett.* **70** 57–59